

Fluid inertia is an effective gyrotactic mechanism for settling elongated micro-swimmers

Jingran Qiu,¹ Zhiwen Cui,¹ Eric Climent,² and Lihao Zhao^{1,*}

¹*AML, Department of Engineering Mechanics, Tsinghua University, 100084 Beijing, China*

²*Institut de Mécanique des Fluides de Toulouse (IMFT), UMR5502 Université de Toulouse, CNRS. Allée du Prof. Camille Soula – 31400 Toulouse, France*

(Dated: Nov. 2nd, 2020)

Gyrotaxis, which helps swimming marine plankton to stabilize upward orientation, is essential for their vertical migration through the water column. There are three classical mechanisms for gyrotaxis: bottom-heaviness, fore-aft asymmetry of plankton shape, and active movement by using a gravity receptor. Here, we discover a gyrotactic mechanism arising from the effect of fluid inertia for settling elongated micro-swimmers. Fluid inertia influences swimmers' rotation when they swim relative to the local fluid with a velocity that is comparable to the local fluid velocity scale. When swimming velocity is greater than the settling speed, swimmers tend to swim in the direction opposite to gravity. Our results reveal the importance of fluid inertia on settling micro-swimmers, and also indicate that settling effect is nontrivial even if a swimmer swims much faster than it settles. By direct numerical simulations, we examine the statistics of the orientation and spatial clustering of cells in both quiescent and turbulent flows. A power law between the mean swimming direction and the swimming and settling velocities is observed in turbulence. We also demonstrate how fluid inertia enhances the gyrotaxis of plankton chains. Enhanced preferential orientation in the opposite direction to gravity reinforce the upward migration to the turbulent upper layer of the ocean.

Keywords: swimmer, turbulence, gravitaxis, fluid inertia

* zhaolihao@mail.tsinghua.edu.cn

INTRODUCTION

Plankton are unicellular micro-organisms that live in ocean, lakes, and rivers. Plankton exert a profound influence on regional and global processes because of their tremendous numbers. Phytoplankton, for example, produce about half of Oxygen on earth and participate in the Carbon cycle (1, 2). Plankton are the base of the marine food web and directly control the productivity of the marine ecosystem. Small in size, many plankton species are motile and can swim vigorously in order to promote nutrient uptake, mating or escape from predators (3–6). Plankton cells in the ocean are experiencing turbulent flow environment thanks to wind shear, large scale water currents and flow instability due to thermal convection. Plankton motility is biased such that cells swim in a vertical direction, allowing them to spend the daylight hours near the surface, where light is stronger, and spend the night in the deep water column, where nutrients are more abundant (3). To accomplish this directed motion, many motile plankton acquire a gravitactic stabilizing torque due to gravity that tends to keep cells swimming in the upward direction. When gravitaxis is combined to orientation response to local flow gradients in the ambient fluid, the instantaneous swimming orientation of the cell is dictated by a mechanism known as gyrotaxis.

Gyrotaxis is an important trait that provides plankton with stability in the orientation opposite to gravity. As a major mechanism that drives vertical migration (7), gyrotaxis determines the migration direction and efficiency (8–10). The gyrotactic effect on swimming plankton in turbulence has been widely studied over the past decade. Durham et al. (9) explained the formation of thin layers of plankton under fluid shear by considering plankton cells as spherical gyrotactic swimmers. Durham et al. (11) reported that gyrotactic plankton cells swimming in turbulence show fractal clustering and sample preferentially downwelling regions where clustering is intense. On the basis of these pioneer studies, researchers consider more realistic factors that influence the motion, orientation, and clustering of swimming plankton in turbulence. Fluid acceleration was reported to generate clusters of gyrotactic swimmers, especially in high-vorticity regions (12). Chain formation of gyrotactic swimming plankton was found to accelerate the daily vertical migration (8). The elongated shape of plankton cells weakens the alignment of swimming direction with the gravity direction (13), and changes the degree of fractal clustering and preferential sampling (14, 15). The effects of wind, thermal convection, and multi-scale flow fluctuations on gyrotactic plankton in wall-bounded turbulence were also studied (16–18). These studies showed that gyrotactic stability has a remarkable influence on the clustering and vertical migration of plankton cells, which may have a strong impact on their growth, predation, and reproduction (3, 6).

Earlier studies proposed three mechanisms for the gyrotactic stability. The first mechanism is due to an inhomogeneous density distribution within the plankton cell referred to as bottom-heaviness, which is observed on biflagellate species such as *Chlamydomonas* or *Dunaliella* (19). The bottom-heaviness produces an offset between the center of hydrodynamic force and the center of gravity force on a plankton cell, and the offset results in a gravity-induced torque that tends to rotate the swimming cell towards the upward orientation. The second mechanism is caused by the fore-aft asymmetry of plankton cells, which is also observed on *Chlamydomonas* (20, 21). The drag on a settling cell body is smaller than that on the flagella in front of the cell, so another type of torque is generated and rotates the cell. The third mechanism is that some species are suspected to have a gravity receptor that could sense the gravity direction so that they can actively adjust the swimming direction (22–25). For example, *Euglena* and *Paramecium* use mechanosensitive ion channel to detect the pressure on cell membrane caused by gravity (25, 26). The first two mechanisms, which are complementary and equally important (20), have been considered in the model of gyrotactic micro-swimmers.

Many of previous studies used an inertia-less pointwise particle model to describe the motion of a plankton cell, which neglects the fluid inertia effect. Recent studies indicated that even a tiny spheroidal particle is experiencing a fluid inertial torque that affects its orientation when there is a velocity difference between the particle and the local fluid (27–29). Theoretical study of fluid inertial torque on a spheroidal particle settling in a still fluid was conducted in the limits of particle Reynolds number $Re_p = |\mathbf{u} - \mathbf{v}_p|L/\gamma \ll 1$ (29, 30). Here, \mathbf{u} and \mathbf{v}_p are the velocities of fluid and particle, respectively, L is the particle length scale, and γ is the kinematic viscosity of fluid. The fluid inertial force, which influences particle translation, is safely neglected with $Re_p \ll 1$ (31), but the fluid inertial torque may still remarkably affects particle orientation in such case. For instance, numerical studies (27, 28) showed that prolate (oblate, resp.) particles with $Re_p \ll 1$ in isotropic turbulence settle with their symmetry axis being perpendicular (parallel, resp.) to the direction of gravity. The fluid inertial torque may also influence swimming plankton's orientation, because motility always results in a slip velocity between the plankton cell and the local fluid. As shown in section of *Model of swimmers with fluid inertia effect*, the magnitude of fluid inertia effect on the rotation of a plankton cell is comparable to the effect of velocity gradient of turbulence in some realistic flow configurations. However, the fluid inertia effect on a settling micro-swimmer, such as plankton, is still veiled. What is the effect of fluid inertia on the orientation statistics of micro-swimmers? Under which circumstances does the fluid inertia matter? To answer these questions, we investigate the effect of fluid inertial torque on elongated settling micro-swimmers in homogeneous isotropic turbulence. We discover that the combination of swimming and settling effects of

an elongated particle results in an interesting original mechanism of gyrotaxis for swimmers. In the present study, we first discuss the inertia-less point particle model for realistic plankton species. Secondly, we analyze how an elongated cell orients its swimming direction in a quiescent flow under the fluid inertial torque. We also discuss how orientation and clustering statistics of swimmers are altered by fluid inertia in homogeneous isotropic turbulence. Finally, we demonstrate and explain how fluid inertia enhances gyrotactic stability of plankton chains, which is beneficial to upward migration.

RESULT AND DISCUSSION

Model of micro-swimmers with fluid inertia effect

In the present study, plankton cells are modeled as point-wise elongated swimmers experiencing turbulent fluid motion (8, 9, 11, 13, 14). Particle inertia is quantified by the Stokes number $St = \tau_p/\tau_\eta$, where τ_p is the particle relaxation time (32, 33), and τ_η is the Kolmogorov time scale. The particle relaxation time, $\tau_p \sim \rho^* L^2/\gamma$, is a measure of the time for a particle to respond to fluid velocity fluctuations and it scales with the particle-to-fluid density ratio ρ^* (which is only a few percent above one for plankton cells), the typical length scale L of the swimmer, and the kinematic viscosity of sea water γ . In flows with $St < 0.1$, the hydrodynamic torque and force on a particle are negligible (28). Therefore, the swimmer's rotation and translation are governed by the following equations:

$$\dot{\mathbf{n}} = \boldsymbol{\omega}_p \times \mathbf{n}, \quad (1)$$

$$\mathbf{v}_p = \mathbf{u} + v_{swim} \mathbf{n} + \mathbf{v}_{settle}, \quad (2)$$

where \mathbf{n} is the unit vector along the particle symmetry axis, and $\boldsymbol{\omega}_p$ is the angular velocity of the swimmer. The swimmer is assumed to swim at a constant velocity along the symmetry axis, e.g. $v_{swim} \mathbf{n}$, relative to the fluid, while it is also advected by the local fluid flow with velocity \mathbf{u} . Settling due to gravity is taken into account by adding a settling speed \mathbf{v}_{settle} . With negligible particle inertia, particle settling in a fluid flow satisfies the Stokesian flow assumption with $Re_p \ll 1$, and the settling speed is expressed as (34, 35):

$$\mathbf{v}_{settle} = -v_1 \mathbf{e}_y - (v_3 - v_1) (\mathbf{e}_y \cdot \mathbf{n}) \mathbf{n}, \quad (3)$$

where v_1 and v_3 are the Stokes settling velocities of a prolate spheroid in a quiescent fluid with its symmetry axis being orthogonal to and parallel to the gravity direction, respectively. In the present study, we specify the direction of y -axis \mathbf{e}_y as the direction opposite to gravity, i.e. $\mathbf{e}_y = -\mathbf{g}/|\mathbf{g}|$. Figure 1(a-c) shows a sketch of such a settling swimmer and the notations used in the Cartesian frame of reference. To characterize the settling effect, we define $V_{settle} = (2v_1 + v_3)/3$ as the mean settling velocity of randomly-oriented particles in a quiescent fluid.

The particle angular velocity is governed by (28):

$$\begin{aligned} \boldsymbol{\omega}_p = & \boldsymbol{\omega} + \Lambda (\mathbf{n} \times \mathbf{S} \cdot \mathbf{n}) + \frac{1}{2B} (\mathbf{n} \times \mathbf{e}_y) \\ & + \frac{M}{\gamma} [\mathbf{n} \cdot (\mathbf{v}_p - \mathbf{u})] [\mathbf{n} \times (\mathbf{v}_p - \mathbf{u})]. \end{aligned} \quad (4)$$

Here, the first two terms on the right-hand-side yield the classical *Jeffery orbits* (36), which represent the contributions of local fluid vorticity $\boldsymbol{\omega}$ and strain rate \mathbf{S} , respectively. The elongation factor $\Lambda = (\lambda^2 - 1) / (\lambda^2 + 1)$, which varies from 0 for spheres to 1 for infinitely elongated rods, characterizes the elongation of swimmers' shape. Here, λ is the aspect ratio, defined as the ratio between the lengths of major and minor axes of a prolate spheroidal particle. The third term represents the effect of gyrotaxis ascribed to bottom-heaviness and fore-aft asymmetry. Here, B is the reorientation time scale for a particle to restore its upward orientation under the gyrotactic torque, and B is inversely proportional to the gyrotactic stability (19–21). The forth term is the *fluid inertia term*. The shape factor M , which only depends on λ , is always negative for prolate spheroids (see section of *Methods* and Figure 8). Replacing \mathbf{u} and \mathbf{v}_p in Eq. 4 with Eqs. 2 and 3, we obtain a expression of angular velocity for settling elongated swimmers including the contribution of fluid inertial torque:

$$\begin{aligned} \boldsymbol{\omega}_p = & \boldsymbol{\omega} + \Lambda (\mathbf{n} \times \mathbf{S} \cdot \mathbf{n}) + \frac{1}{2B} (\mathbf{n} \times \mathbf{e}_y) \\ & + \frac{M}{\gamma} [v_{swim} v_1 (\mathbf{e}_y \times \mathbf{n}) - v_1 v_3 (\mathbf{e}_y \cdot \mathbf{n}) (\mathbf{e}_y \times \mathbf{n})]. \end{aligned} \quad (5)$$

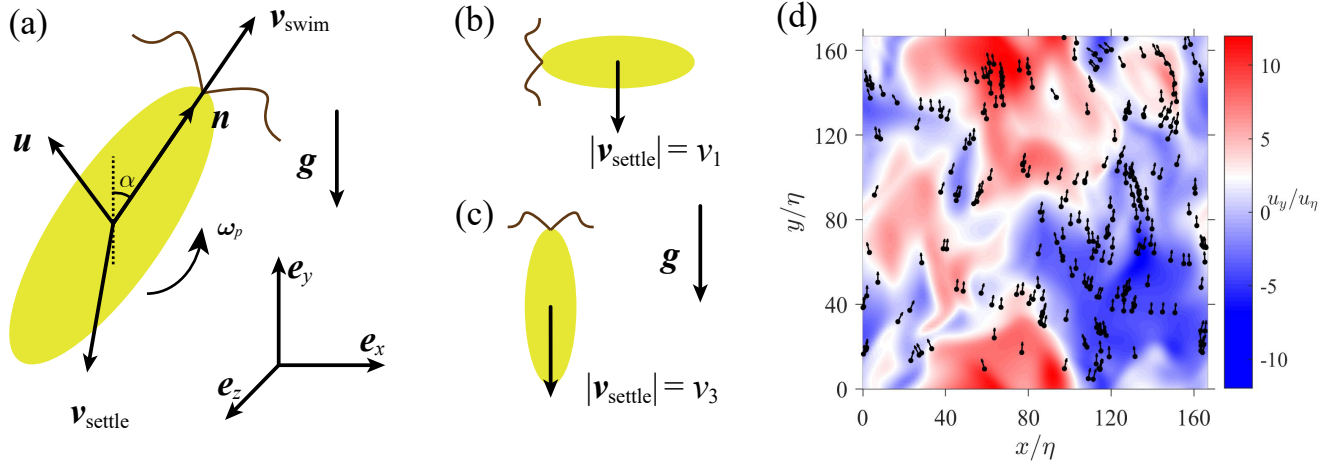


FIG. 1. Sketch of settling micro-swimmers and instantaneous distribution of swimmers in turbulence. (a) Sketch of a settling elongated swimmer. \mathbf{e}_x , \mathbf{e}_y , and \mathbf{e}_z are the base vectors of the global frame of reference. (b) A particle settling with the symmetry axis perpendicular to gravity. (c) A particle settling with its symmetry axis parallel to the direction of gravity. (d) Instantaneous spatial distribution of swimmers in homogeneous isotropic turbulence. Black dots and tiny arrows stand for the position and swimming direction of each swimmer, respectively. Colors represent the normalized vertical fluid velocity u_y/u_η . η is the Kolmogorov length scale of turbulence. To isolate the effect of fluid inertia, gyrotaxis due to bottom-heaviness or fore-aft asymmetry is removed by setting $B = \infty$. The parameters of micro-swimmers in the simulation are: $\lambda = 4$, $\phi_{\text{settle}} = 0.5$, $\phi_{\text{swim}} = 10$, corresponding to $\omega_{\text{inert}}/\omega_{\text{Jeff}} = 0.68$.

Here, the fluid inertia term on the right-hand-side consists of two parts. We refer to $\frac{M}{\gamma} v_{\text{swim}} v_1 (\mathbf{e}_y \times \mathbf{n})$ as the *swim-settling term* because it arises from the coupling of swimming and settling. We refer to $-\frac{M}{\gamma} v_1 v_3 (\mathbf{e}_y \cdot \mathbf{n}) (\mathbf{e}_y \times \mathbf{n})$ as the *settling term*, which is ascribed to settling only.

The present particle model neglects both particle and fluid inertia effects on the translational motion (31). Particle inertia is neglected because Stokes number is much smaller than unity (28, 37), and fluid inertia on particle translation is neglected as $\text{Re}_p \ll 1$. However, for the rotation, the effect of fluid inertia needs to be considered (28) and the present study highlight the crucial role of fluid inertial contribution to orientational dynamics. Plankton swimming gaits are usually referred to either pusher or puller. The cell motion that produces the propulsion force will disturb ambient fluid, which may change the hydrodynamic force and torque on the swimmer. Actually, this effect has been implicitly neglected in earlier studies (8, 11, 13–15, 38), which assume that the Jeffery torque on a swimmer is the same as that on a non-motile particle. These studies have successfully explained the phenomena observed in laboratory experiments and field measurements. Hence, following those guidelines, we neglect any disturbance effect due to the propulsion behavior on the hydrodynamic force and torque on a swimmer. In such case, the fluid inertia torque is only ascribed to the slip velocity between the swimmer and fluid.

In Eq. 5, the ratio between the magnitude of fluid inertia term, $\omega_{\text{inert}} = \left| \frac{M}{\gamma} [v_{\text{swim}} v_1 (\mathbf{e}_y \times \mathbf{n}) - v_1 v_3 (\mathbf{e}_y \cdot \mathbf{n}) (\mathbf{e}_y \times \mathbf{n})] \right|$, and the Jeffery term, $\omega_{\text{Jeff}} = |\boldsymbol{\omega} + \boldsymbol{\Lambda}(\mathbf{n} \times \mathbf{S} \cdot \mathbf{n})|$, shows the importance of fluid inertia relative to the fluid velocity gradients. Fluid inertia effect is contributed by both the swimming-settling and the settling terms. Considering that the swimming velocity is usually much greater than the settling velocity for plankton (see Table I), we only use the swimming-settling term in the estimate, i.e. $\omega_{\text{inert}} \sim |M| v_{\text{swim}} v_1 / \gamma$. The Jeffery term, $\omega_{\text{Jeff}} \sim u_\eta / \eta$ gives an estimate of the fluid gradient experienced by small size particles in turbulence (u_η is the Kolmogorov velocity scale and η the corresponding length scale). Using $\gamma = u_\eta / \eta$ and $v_1 \approx V_{\text{settle}}$, we obtain $\omega_{\text{inert}}/\omega_{\text{Jeff}} \sim |M| \Phi_{\text{swim}} \Phi_{\text{settle}}$, where $\Phi_{\text{swim}} = v_{\text{swim}}/u_\eta$ and $\Phi_{\text{settle}} = V_{\text{settle}}/u_\eta$ are the *swimming* and *settling numbers*, respectively. Fluid inertia cannot be neglected when $\omega_{\text{inert}}/\omega_{\text{Jeff}}$ is close to or larger than unity, i.e. when the product of swimming and settling numbers is greater than unity. The fluid inertia term promotes swimmer's alignment in a certain direction with respect to the gravity direction (as shown in the section of *Settling swimmers in turbulence*), while the Jeffery term randomizes angular velocity due to fluctuations of velocity gradients in turbulence. Therefore, in the long term integration of Eq. 5, the effect of Jeffery terms may vanish, and the fluid inertia term dominates the orientation of swimmers. For instance, Figure 1(d) shows an instantaneous distribution of swimmers at $\omega_{\text{inert}}/\omega_{\text{Jeff}} = 0.68$ without including gyrotaxis caused by bottom-heaviness or fore-aft asymmetry. Swimmers apparently orient in upward direction and exhibit clustering under the fluid inertia effect. Tables I and II show the parameters of some typical plankton species. A plankton swimming in oceanic turbulence falls in the limits of $\text{St} < 0.1$ and $\text{Re}_p \ll 1$, so the

TABLE I. Parameters of typical plankton species (4, 39–42).

Species		Width(μm)	Length(μm)	λ	v_{swim} (μm/s)	V_{settle} (μm/s)
Cochlodinium polykrikoides (39)	single cell	25.1 ± 2.7	40.8 ± 2.0	1.63 ± 0.25	391 ± 92	26 ¹
	2-cells	25.3 ± 1.8	50.7 ± 0.9	2.00 ± 0.18	599 ± 126	29 ¹
	4-cells	25.5 ± 0.7	102.3 ± 4.2	4.01 ± 0.27	800 ± 129	42 ¹
	8-cells	29.0 ± 1.4	182.0 ± 10.9	6.28 ± 0.68	856 ± 108	65 ¹
Centropages typicus (41, 42)	early nauplius	57.0 ± 11.5	132.0 ± 16.0	2.31 ± 0.19	330 ± 210	50 ± 40
	late nauplius	97.2 ± 22.1	225.0 ± 33.0	2.31 ± 0.19	720 ± 310	140 ± 70
Euterpina acutifrons (41)	late nauplius	86.6 ± 18.7	200.0 ± 27.0	—	1080 ± 310	260 ± 50
Eurytemora affinis (41)	late nauplius	87.4 ± 18.7	202.0 ± 27.0	—	1640 ± 400	182
Temora longicornis (40, 41)	late nauplius	133.3 ± 26.3	308.0 ± 36.0	—	570 ± 140	240 ± 70
	copepod	129.0 ± 26.8	298.0 ± 38.0	—	820 ± 180	170 ± 240
Ceratium tripos (4)	—	73.5	—	—	167	164
Ceratium furca (4)	—	45.1	—	—	780	62
Akashiwo sanguinea (4)	—	42.2	—	—	300	54
Dinophysis acuminata (4)	—	32.4	—	—	332	32
Alexandrium minutum (4)	—	18.1	—	—	278	10
Prorocentrum minimum (4)	—	12.7	—	—	206	5

^a Data are mean values ± standard deviations. —: unavailable data. Superscript¹: V_{settle} is calculated using Stokes settling velocity assuming that the density of *Cochlodinium polykrikoides* is 5.9% greater than fluid density (43).

TABLE II. Dimensionless numbers of typical plankton species shown in Table I (4, 39–42).

Species	Φ_{swim}	Φ_{settle}	M	Re_p	$St(\times 10^{-5})$	$\omega_{inert}/\omega_{Jeff}$
Cochlodinium polykrikoides (39)	single cell	2.17 ~ 0.39	0.14 ~ 0.03	-0.078	0.015	0.15 ~ 4.59
	2-cells	3.32 ~ 0.59	0.16 ~ 0.03	-0.101	0.029	0.17 ~ 5.28
	4-cells	4.44 ~ 0.79	0.23 ~ 0.04	-0.136	0.077	0.24 ~ 7.51
	8-cells	4.75 ~ 0.84	0.36 ~ 0.06	-0.137	0.147	0.37 ~ 11.61
Centropages typicus (41, 42)	early nauplius	1.83 ~ 0.33	0.28 ~ 0.05	-0.114	0.041	0.92 ~ 28.98
	late nauplius	3.99 ~ 0.71	0.78 ~ 0.14	-0.114	0.153	2.66 ~ 84.20
Euterpina acutifrons (41)	late nauplius ¹	5.99 ~ 1.06	1.44 ~ 0.26	-0.114	0.204	2.10 ~ 66.53
Eurytemora affinis (41)	late nauplius ¹	9.09 ~ 1.62	1.01 ~ 0.18	-0.114	0.313	2.15 ~ 67.87
Temora longicornis (40, 41)	late nauplius ¹	3.16 ~ 0.56	1.33 ~ 0.24	-0.114	0.166	4.99 ~ 157.78
	copepod ¹	4.55 ~ 0.81	0.94 ~ 0.17	-0.114	0.231	4.67 ~ 147.70
Ceratium tripos ² (4)	—	0.93 ~ 0.16	0.91 ~ 0.16	-0.101	0.012	0.35 ~ 11.10
Ceratium furca ² (4)	—	4.32 ~ 0.77	0.34 ~ 0.06	-0.101	0.033	0.13 ~ 4.18
Akashiwo sanguinea ² (4)	—	1.66 ~ 0.30	0.30 ~ 0.05	-0.101	0.012	0.12 ~ 3.66
Dinophysis acuminata ² (4)	—	1.84 ~ 0.33	0.18 ~ 0.03	-0.101	0.010	0.07 ~ 2.16
Alexandrium minutum ² (4)	—	1.54 ~ 0.27	0.05 ~ 0.01	-0.101	0.005	0.02 ~ 0.67
Prorocentrum minimum ² (4)	—	1.14 ~ 0.20	0.03 ~ 0.00	-0.101	0.002	0.01 ~ 0.33

^a The Kolmogorov scales of ocean turbulence is calculated with $\gamma = 1.058 \times 10^{-6} \text{ m}^2 \text{s}^{-1}$, and dissipation rate ϵ is ranging from 1×10^{-9} to $1 \times 10^{-6} \text{ m}^2 \text{s}^{-3}$ (44). Re_p is calculated with $Re_p = v_{swim} L / \gamma$ because $v_{swim} > V_{settle}$ for many species in Table I. Superscript¹: The values are calculated with $\lambda = 2.3$ similar to *Centropages typicus*. Superscript²: The values are calculated with $\lambda = 2.00$.

present particle model is justified. $\omega_{inert}/\omega_{Jeff}$ is smaller than unity for most of these species, but species with high motility have $\omega_{inert}/\omega_{Jeff}$ close to unity, especially in weak turbulence. Therefore, the fluid inertia effect on swimming plankton must be considered as a dominant physical mechanism on the long term overall dynamics.

Settling swimmers in a quiescent fluid

First, we consider settling swimmers without bottom-heaviness and fore-aft asymmetry corresponding to $B = \infty$. According to Eq. 5, the angular velocity of particle in a quiescent fluid is only affected by fluid inertia as follows:

$$\boldsymbol{\omega}_p = \frac{M}{\gamma} [v_{swim} v_1 (\mathbf{e}_y \times \mathbf{n}) - v_1 v_3 (\mathbf{e}_y \cdot \mathbf{n})(\mathbf{e}_y \times \mathbf{n})]. \quad (6)$$

Here, the swimming-settling term rotates elongated particles to swim upwards (i.e., opposite to gravity) because M is negative for prolate particles, whereas the settling term tends to align the spheroid horizontally (i.e., with symmetry

axis perpendicular to gravity). These two terms are competing, and the stable orientation of a settling swimmer in a quiescent fluid depends on the relative contribution of swimming and settling velocities. We use a linear stability theory to analyze the stable swimming direction. In a quiescent fluid, the ω_p vector must be perpendicular to the plane spanned by \mathbf{n} and \mathbf{e}_y , so the rotation of a swimmer can be described by an angle α which is defined as the angle of \mathbf{n} relative to \mathbf{e}_y (see Figure 1(a)). Therefore, we rewrite Eq. 6 in the form of:

$$\frac{d\alpha}{dt} = \frac{M}{\gamma} (v_{swim} v_1 \sin \alpha - v_1 v_3 \cos \alpha \sin \alpha). \quad (7)$$

Thus, the swimmer has three equilibrium orientations:

$$\alpha_0^{(1)} = 0, \quad \alpha_0^{(2)} = \arccos \frac{v_{swim}}{v_3}, \quad \alpha_0^{(3)} = \pi, \quad (8)$$

which correspond to a particle (1) swimming upward against gravity, (2) swimming with a fixed angle with respect to gravity direction, and (3) swimming downward along gravity, respectively. Derived from Eq. 7, the first order linear equation of a small perturbation around the equilibrium orientations, $\delta\alpha$, reads:

$$\frac{d\delta\alpha}{dt} = \frac{M v_1 v_3}{\gamma} (R_v \cos \alpha_0 - \cos 2\alpha_0) \delta\alpha, \quad (9)$$

where we use the Tayler expansion around α_0 and neglect the $o(\delta\alpha)$ terms, and $R_v = v_{swim}/v_3$. An equilibrium orientation is stable as long as any small perturbation decays in time, which means the prefactor in front of $\delta\alpha$ on the right-hand-side of Eq. 9 is negative. Since M is negative for prolate particles, $\alpha_0^{(3)}$ is always unstable, but the stability of $\alpha_0^{(1)}$ and $\alpha_0^{(2)}$ depends on R_v . In general, the vertical component of the swimming direction at stable orientation is as follows:

$$n_y \equiv \mathbf{n} \cdot \mathbf{e}_y = \cos \alpha_0 = \min(1, R_v). \quad (10)$$

A swimmers has only one stable orientation under any circumstances. When $R_v < 1$, the swimming-settling term does not overcome the settling term, so the swimmer reaches an intermediate orientation where the two terms balanced. $n_y = \cos \alpha_0^{(2)}$ of the equilibrium point increases monotonously with R_v . However, when $R_v > 1$, the swimming-settling term overcomes the settling term for any orientation, so the swimmer rotates to swim upward. In such case, fluid inertia produces an effective gyrotaxis for the settling swimmer. Simulations in a quiescent fluid are performed to compare with the theoretical analysis. Settling elongated swimmers are released with random orientation initially, and their orientation gradually evolves toward the theoretical equilibrium points after a transient time (Figure 2). According to Eq. 9, we define $\tau_{trans} = \gamma/|M| v_1 v_3$ as a time scale for the transient regime. Mean orientation of swimmers converges in a short time when $R_v > 1$, but takes a longer transient time to converge when $R_v < 1$. The transient time is the longest in the critical case of $R_v = 1$, because the swimming-settling term and settling term are almost balanced when $n_y \approx 1$, resulting in a small particle angular velocity.

Settling swimmers in turbulence

In this section, we consider settling swimmers without bottom-heaviness or fore-aft asymmetry ($B = \infty$) in homogeneous isotropic turbulence, and the swimmers' rotation is subjected to both fluid velocity gradients and fluid inertia (Eq. 4). Considering the typical parameters of plankton in ocean turbulence (4, 8, 10, 39–46), we investigate swimmers with a parameter space of $\Phi_{swim} = 0 \sim 10$, $\Phi_{settle} = 0 \sim 1$, and $\lambda = 1 \sim 8$. First, we examine the shape effect on the orientation of swimmers. As shown in Figure 3(a), spherical swimmers show no preferential orientation with regards to gravity and tumble with random orientation because fluid velocity gradients remain isotropic and fluid inertia effect vanishes ($M = 0$). However, elongated swimmers show preferential alignment due to fluid inertia effect. When $\Phi_{swim} = 0$, settling elongated particles are aligned perpendicular to the direction of gravity as reported in earlier studies (27, 28, 47). The alignment is weak because of the negligible fluid inertia effect for small Φ_{settle} , so the fluid velocity gradients dominate the particle angular velocity and randomizes the orientation. With increasing Φ_{swim} , elongated swimmers tend to swim in the upward direction (Fig. 3b-d), and a strong preferential alignment is observed when Φ_{swim} is greater than unity. Figure 3(d) shows that $\langle n_y \rangle$ monotonously increases as λ grows and saturates at $\lambda = 8$. Therefore, we choose $\lambda = 8$ as a representative aspect ratio which embodies the nature of prolate swimmers, and focus on the effects of Φ_{swim} and Φ_{settle} .

Probability distribution functions (PDFs) of n_y of elongated swimmers ($\lambda = 8$) corresponding to different Φ_{swim} are shown in Figure 4(a). Due to the random fluctuations of turbulence, the peaks of PDFs do not perfectly match

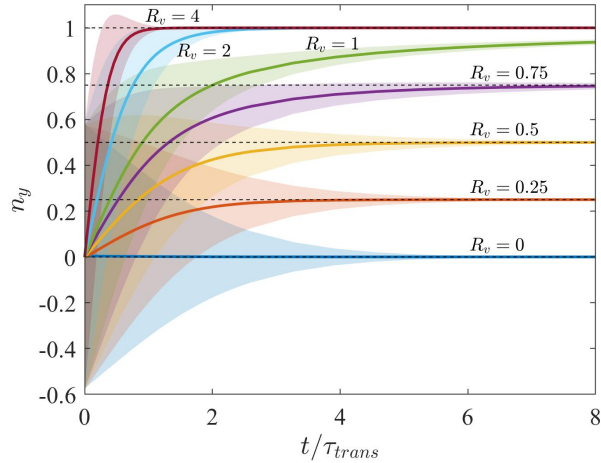


FIG. 2. Vertical components of the swimming direction, n_y , versus dimension-less time t/τ_{trans} in a quiescent fluid. The solid lines represent the mean value of n_y , and the colored areas represent the ranges of mean \pm standard deviation. Horizontal dashed lines stand for the theoretical equilibrium orientation. The aspect ratio of swimmers is $\lambda = 8$ for all cases here.

the stable orientations observed in the case of quiescent fluid (dashed lines) for $0 < R_v < 1$. However, the peak locations shift to the right as Φ_{swim} increases, qualitatively in agreement with the quiescent fluid case. Figure 4(b) shows that the mean n_y augments with increasing Φ_{settle} or Φ_{swim} monotonously. Interestingly, we observe a power law $\langle n_y \rangle \propto \Phi_{swim}\Phi_{settle}$ when $\Phi_{swim}\Phi_{settle} < 1$. However, the physics yielding this power law is complicated because the mean orientation results from three different contributions. The fluctuations of fluid velocity gradients tend to randomize the particle orientation, the swimming-settling term due to fluid inertia tends to align particles in upward direction, while the settling term of fluid inertia tends to align particles perpendicular to gravity. As discussed in the Section of *Model of swimmers with fluid inertia*, the relative influence of fluid inertia to fluid velocity gradients is evaluated by $\omega_{inert}/\omega_{Jeff} \sim |M|\Phi_{swim}\Phi_{settle}$ if $\Phi_{swim} \gg \Phi_{settle}$. Therefore, a qualitative explanation for this power law is that the swimming-settling term due to fluid inertia provides a stronger effective gyrotactic stability as $\Phi_{swim}\Phi_{settle}$ increases, which results in a greater $\langle n_y \rangle$ under the competition with turbulent velocity gradients. This argument may provide a convenient way to estimate $\langle n_y \rangle$ using Φ_{swim} and Φ_{settle} in homogeneous isotropic turbulence.

We quantify the clustering of swimmers by Voronoi tessellation of the simulation domain based on particle position, which is an approach to measure the inhomogeneity of particle spatial distribution (48, 49). A larger variance of Voronoi volumes indicates stronger clustering of the plankton cells. As shown in Figure 5(a), spherical swimmers, without influence of fluid inertia, show no clustering in accordance with the literature (13), whereas elongated swimmers show strong clustering under fluid inertia effect. As reported in earlier studies (13, 15), with weak gyrotactic stability the clustering is stronger on elongated swimmers than spherical ones, but when the stability enhances, the clustering of elongated swimmers is weaker than that of spherical ones. The magnitude of gyrotactic stability ascribed to fluid inertia is proportional to $\Phi_{swim}\Phi_{settle}$ at $\Phi_{swim} > \Phi_{settle}$. When $\Phi_{swim} < 3$, fluid inertial gyrotactic stability is weak, so the most elongated swimmers experience the strongest clustering. When $\Phi_{swim} > 3$, spherical swimmers do not obtain stability from fluid inertia and thus, show no clustering, whereas elongated swimmers obtain strong stability. Therefore, swimmers that are less elongated, e.g. those with $\lambda = 2$, show stronger clustering than more elongated swimmers. Figure 5(b) indicates that the variance of Voronoi volumes increases monotonously as Φ_{settle} grows when $\Phi_{swim} < 5$, but the trend becomes non-monotonic at large Φ_{swim} . When Φ_{settle} increases from zero to unity, the stability of fluid inertial gyrotaxis increases from zero to a high level due to large Φ_{swim} . Elongated swimmers with large Φ_{swim} form the most dense clusters when the stability has moderate intensity (13, 15), explaining why the maximal clustering is observed at an intermediate Φ_{settle} .

Figure 5 (c, d), presented the statistics on the vertical fluid velocity, u_y , sampled by particles. Figure 5(c) indicates that spherical swimmers do not show any preferential sampling. However, elongated swimmers with moderate values of Φ_{swim} and λ sample downwelling regions, while they switch to sample upwelling regions as Φ_{swim} and λ increase. This behavior is in agreement with earlier observations (8, 15). Figure 5 (d) shows the mean vertical velocity $\langle u_y \rangle$ sampled by prolate swimmers over the parameter space of Φ_{swim} and Φ_{settle} . $\langle u_y \rangle$ increases with Φ_{swim} almost monotonously for small Φ_{settle} . However, a significant drop of $\langle u_y \rangle$ toward negative values is observed when $\Phi_{swim} \simeq 3$ and $\Phi_{settle} > 0.2$. This response of swimmers is due to an enhanced gyrotactic stability induced by fluid inertia, which

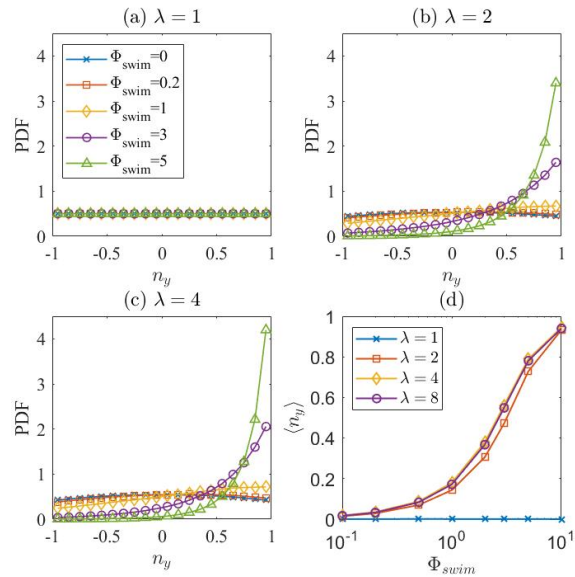


FIG. 3. Alignment of swimmers in upward direction with $\Phi_{settle} = 0.5$. (a, b, and c): The probability distribution functions (PDFs) of n_y of particles with $\lambda = 1, 2$, and 4 , respectively. (d): $\langle n_y \rangle$ versus Φ_{swim} for different aspect ratios, where $\langle \cdot \rangle$ denotes the ensemble average.

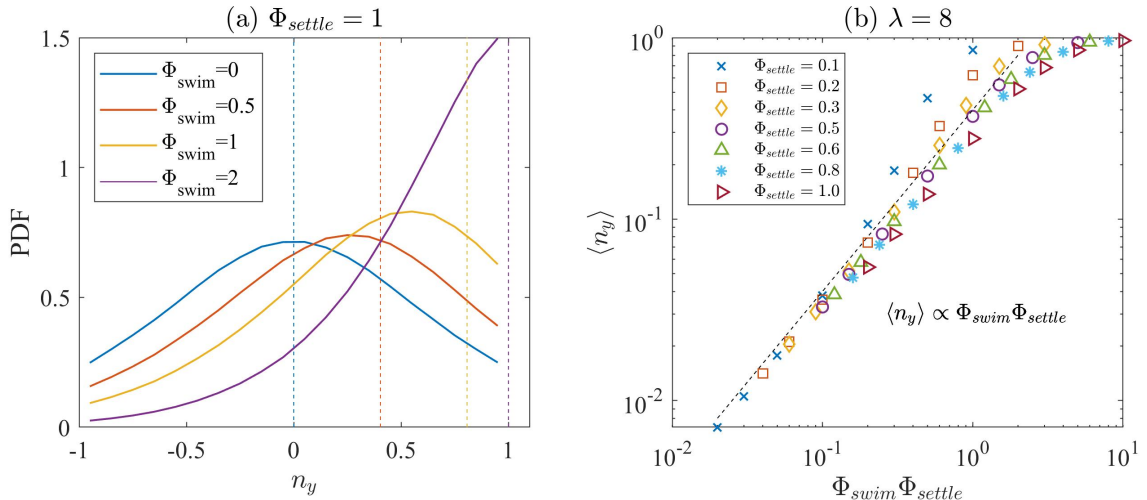


FIG. 4. Alignment of swimmers in upward direction with $\lambda = 8$. (a): PDFs of n_y of swimmers with $\Phi_{settle} = 1$ in turbulence. Vertical dashed lines represent the equilibrium points predicted by Eq. 10. Four dashed lines from left to right correspond to $\Phi_{swim} = 0, 0.5, 1$, and 2 , respectively. (b) $\langle n_y \rangle$ versus $\Phi_{swim}\Phi_{settle}$ with $\lambda = 8$.

makes swimmers preferentially sample the downwelling flows with the swimming velocity smaller than the typical velocity scale of fluctuations in turbulence (15). That is observed only in the case with large Φ_{settle} , for which the effective gyrotactic stability is strong enough to promote preferential sampling of downwelling flows. According to literature (15), the critical Φ_{swim} corresponding to the switch of sampling regions (i.e. $\langle u_y \rangle = 0$) monotonically increases with stronger gyrotactic stability. In our case, stability is originated from fluid inertia, which characterized by $|M| \Phi_{swim} \Phi_{settle}$. Therefore, the critical Φ_{swim} increases with Φ_{settle} as shown in Figure 5(d).

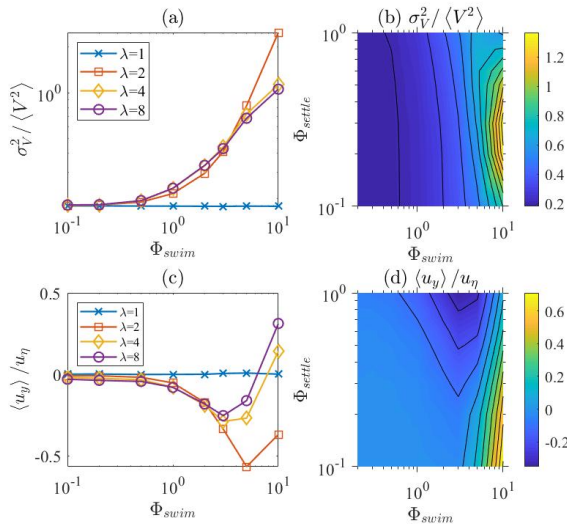


FIG. 5. Statistics of Voronoi volumes and preferential sampling of swimmers in turbulence. (a) Normalized Variance of Voronoi volumes σ_V^2 of swimmers with $\Phi_{settle} = 0.5$, nondimensionalized by the mean square of Voronoi volumes $\langle V^2 \rangle$. (b) Normalized variance of Voronoi volumes of swimmers with $\lambda = 8$. (c) Mean vertical fluid velocity at swimmers' positions with $\Phi_{settle} = 0.5$. (d) Mean vertical fluid velocity at swimmers' positions with $\lambda = 8$.

Fluid inertia effect on bottom-heavy plankton

The analysis of section *Settling swimmers in turbulence* suggests that fast, prolate swimmers obtain an effective gyrotactic stability thanks to fluid inertia. With regards to plankton, the fluid inertia effect may provide extra gyrotactic stability in addition to those ascribed to bottom-heaviness or fore-aft asymmetry. Here, using chains of bottom-heavy plankton cells as an example, we compare the statistics on migration and clustering in the case with and without fluid inertia effect. We consider plankton chains of n cells as elongated spheroids whose lengths of minor and major axes are equal to d and nd , respectively, with d the diameter of a single cell. Bottom-heaviness gyrotaxis corresponds to finite reorientation time, B , in the angular velocity (Eq. 5). For plankton chains, B and v_{swim} are calculated by biological models (8) (see Section of *Methods*), and settling velocity is calculated by the Stokesian terminal settling velocity for spheroids using Eq. 3. When $v_{swim} > v_3$, which usually holds for swimming plankton species (see Table I and references therein), the fluid inertia effect results in gyrotactic stability due to the swimming-settling term in Eq. 5. Noting that the swimming-settling term has a similar form as the gyrotaxis term caused by bottom-heaviness, we define the reorientation time due to fluid inertia, $T_{inert} = \gamma/2|M|v_{swim}v_1$, to evaluate the gyrotactic stability generated by fluid inertia. The factor of 2 in the denominator of T_{inert} is added to be consistent with the definition of gyrotaxis time scale B . We also define the global reorientation time, T_{global} , with $1/T_{global} = (1/T_{inert} + 1/B)$. The angular velocity arises from gyrotaxis is inversely proportional to reorientation time, so a smaller orientation time means a stronger gyrotactic stability. In Table III, we provide the parameters of the plankton chains used in simulations, and we compare the reorientation time of gyrotaxis produced by fluid inertia to bottom-heaviness. As plankton form long chains, v_{swim} , v_1 , and B increase but T_{inert} decreases (8), so the contribution of fluid inertia becomes dominant on the rotation dynamics of long chains. For chains of 8 cells, fluid inertia effect takes up one-third of the global gyrotactic stability (see Table III and Figure 7).

In Figure 6 we compare the statistics of plankton with and without fluid inertia effect in homogeneous isotropic turbulence for typical dissipation rates in ocean turbulence (44). Figure 6(a) indicates that the mean n_y decreases as chain length increases. Longer chains become more sensitive to turbulent vortices, because the global gyrotaxis reorientation time increases (Table III) due to the rapid increase of B for longer chain. However, plankton with fluid inertia effect exhibit stronger upward orientation than the case without fluid inertia, especially for plankton with length ≥ 8 in turbulence where $\epsilon \leq 10^{-8} \text{ m}^2 \text{s}^{-3}$. This is because fluid inertia provides a stronger gyrotactic stability for longer chains that swim faster. Figure 6(b) shows that plankton samples downwelling flows in most cases, which is a typical phenomenon for gyrotactic swimmers with swimming velocity smaller than the root-mean-square velocity of turbulence (15). Plankton with fluid inertia show a stronger non-uniform sampling than those without fluid inertia, because fluid inertia provides extra gyrotactic stability, which results in a stronger sampling of downwelling regions (15). Our result suggests that it is difficult for settling swimming plankton (except those swimming fast in

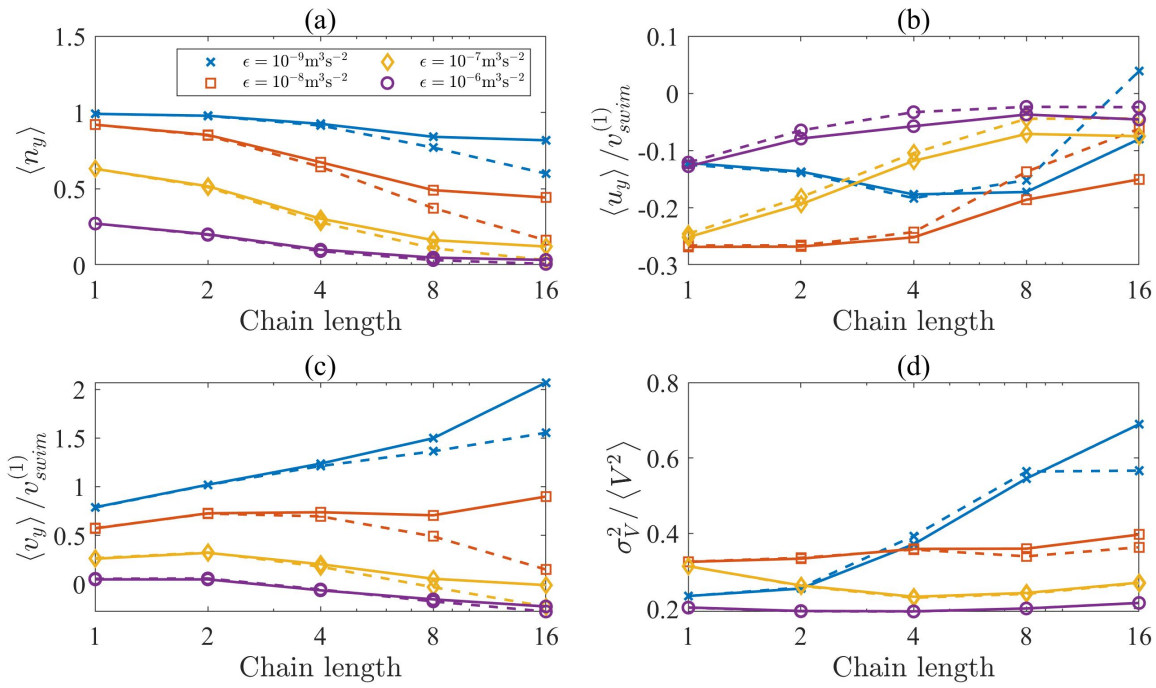


FIG. 6. Statistics of plankton with fluid inertia (solid lines) and without fluid inertia (dashed lines). Different markers represent different turbulence dissipation rates, ϵ . (a) Average alignment in upward direction, $\langle n_y \rangle$. (b) Vertical component of average local fluid velocity $\langle u_y \rangle$ sampled by swimmers normalized by the swimming velocity of a single cell. (c) Average vertical velocity of plankton chains $\langle v_y \rangle$ normalized by the swimming velocity of a single cell. (d) Variance of Voronoi volumes.

the weakest turbulence) to sample upwelling flow. Nevertheless, forming chains helps them to sample downwelling regions with lower intensity than single cells, which is beneficial to upward migration (8). Figure 6(c) shows that the vertical velocity is always positive and is reinforced by forming longer chains for small ϵ . Our results are in agreement with the literature (8), but the mechanisms are more complicated than that in earlier studies. By forming long chains, plankton enhance swimming velocity, but at the same time they settle faster and the global gyrotaxis is weakened. Faster swimming is beneficial to upward migration, while the latter two are detrimental. In weak turbulence, long plankton chains still preserve upward orientation even though the gyrotactic stability is weakened by chain-formation, so the increasing swimming velocity enhances the upward migration. In strong turbulence, however, the orientations of long plankton chains are dominated by fluid velocity gradients and chains are almost randomly orientated, so the increasing swimming velocity does not contribute enough to the upward migration to overcome the disadvantage of increased settling velocity. With fluid inertia effect, plankton chains obtain enhanced gyrotactic stability to compensate for decreased bottom-heavy gyrotaxis. Therefore, the range of ϵ where forming long chains enhances upward migration, is extended from $\epsilon \leq 10^{-9} \text{ m}^2 \text{s}^{-3}$ for plankton without fluid inertia, to $\epsilon \leq 10^{-8} \text{ m}^2 \text{s}^{-3}$ for those with fluid inertia.

We also examine the degree of clustering by statistical analysis of Voronoi volumes. As shown in Figure 6(d), longer chains of plankton experience stronger clustering under weak turbulence, but chain length have negligible effect in more intensive turbulence. Fluid inertia has little influence on clustering. For short chains, the gyrotactic stability due to fluid inertia is negligible compared to that of bottom-heaviness. For long chains, fluid inertia have a drastic influence on T_{global} , but clustering is not sensitive to T_{global} at $\omega_{rms} T_{global} > 1$ for an elongated swimmer (13), where ω_{rms} is the root-mean-square vorticity of turbulence. Therefore, we only observe that fluid inertia modifies clustering significantly in the case of long chains in weak turbulence with $\epsilon \leq 10^{-8} \text{ m}^2 \text{s}^{-3}$.

CONCLUSIONS

Fluid inertia exerts a significant influence on the orientation of swimmers when the slip velocity between swimmer and fluid is comparable to the fluid velocity scale. Different from settling particles which tend to align perpendicular to the gravity direction, elongated settling swimmers tend to rotate and swim in the upward swimming direction

TABLE III. Parameters of plankton chains.

chain length	v_{swim} ($\mu\text{m/s}$)	v_1 ($\mu\text{m/s}$)	v_3 ($\mu\text{m/s}$)	Fluid inertia		Bottom-heaviness		T_{global} (s)
				T_{inert} (s)	percentage	B (s)	percentage	
1	300.0	24.5	24.5	∞	0%	5.0	100%	5.00
2	395.9	35.5	40.7	351.1	2%	7.5	98%	7.37
4	522.3	47.7	61.3	147.5	10%	17.0	90%	15.23
8	689.2	60.2	84.7	89.6	34%	47.0	66%	30.83
16	909.4	72.9	109.4	61.3	70%	143.9	30%	42.99

^a The length of the minor axis is fixed to 15 μm for different chain lengths. The percentages in fluid inertia and bottom-heaviness columns represent the percentages of gyrotactic stability (i.e. the inverse of reorientation time) originated from fluid inertia and bottom-heaviness, respectively.

under the combined effect of swimming and settling in both quiescent fluids and turbulent flows. When the swimming velocity is greater than the settling speed, fluid inertia effect turns out to generate an effective gyrotactic torque. Our finding emphasizes the importance of fluid inertia on the rotation of swimmers, such as long chains of plankton which have large swimming and settling speeds (4, 50). We find that fluid inertia has a similar effect as gyrotaxis caused by bottom-heaviness or fore-aft asymmetry. They share a similar mathematical form as shown in Eq. 5. Therefore, we consider fluid inertia as an effective mechanism of gyrotaxis for the settling swimmers. Unlike bottom heaviness or fore-aft asymmetry which contributes to the rotation dynamics passively (20), gyrotactic stability due to fluid inertia is proportional to swimming velocity and can be tuned by plankton cells. This feature provides a possibility that plankton can actively control the gyrotactic stability by adjusting swimming velocity.

Our results also show that settling effect not only affects the translation of swimmers, but also contributes to their rotation due to fluid inertia. It is demonstrated in previous studies (27–29) that fluid inertial torque is independent of the length of the particle, so the fluid inertia effect cannot be simply neglected even if the swimmer is of small size. From this perspective, the settling effect on motile plankton may be more important than expected. In previous studies concerning plankton in turbulence, the settling effect is often neglected. However, neglecting settling may lead to an underestimation of gyrotactic stability because fluid inertia torque will be zero with the assumption of zero settling speed.

METHODS

Direct numerical simulation of turbulence and swimmers

We use an Eulerian-Lagrangian method to simulate the suspensions of swimming particles in homogeneous isotropic turbulence. The dynamics of fluid phase is resolved in an Eulerian frame, while each individual particle is tracked along the Lagrangian trajectory using local instantaneous flow information at particle position. The unsteady dynamics of incompressible homogeneous isotropic turbulence is directly simulated by solving the Navier-Stokes equations:

$$\frac{\partial \mathbf{u}}{\partial t} + \mathbf{u} \cdot \nabla \mathbf{u} = -\frac{\nabla p_f}{\rho} + \gamma \nabla^2 \mathbf{u} + \mathbf{f}, \quad (11)$$

$$\nabla \cdot \mathbf{u} = 0, \quad (12)$$

where t is the time, \mathbf{u} is the fluid velocity. The symbols p_f and ρ denote the pressure and density of fluid, respectively. The body force term, \mathbf{f} , is an external force to sustain turbulence and balances the rate of viscous dissipation at the Kolmogorov scale. Three-dimensional periodic boundary conditions are applied on all boundaries of the cubic domain with size $(2\pi)^3$. The turbulence Taylor-Reynolds number is $\text{Re}_\lambda = 60$ which is within the observed range of Reynolds number of oceanic turbulence. A pseudo-spectral method is used for solving the Navier-Stokes equations, and the 3/2 rule is utilized to reduce the aliasing error on the nonlinear term. An explicit second-order Adam-Basforth scheme is adopted for time integration of Eqs. 11 and 12 (51). We use 96^3 grid points to resolve the turbulent flow fluctuation down to the smallest dissipative scales. The maximum wave number resolved is about 1.78 times greater than the Kolmogorov wave number to ensure accuracy of resolution at small scales (52). A random flow with an exponent energy spectrum is given as the initial flow field in order to reach a statistical steady state quickly. After turbulence is fully developed, swimmers are released in the flow field with random positions and orientations. Fluid velocity and its gradients in Eqs. 1 and 2 are interpolated by a second-order Lagrangian method at the particle position, using

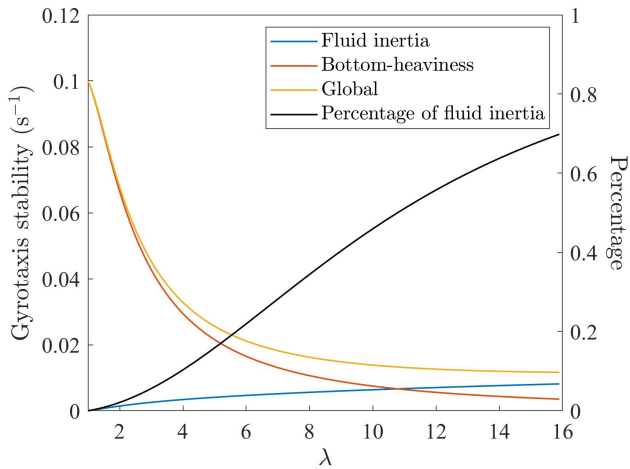


FIG. 7. Gyrotaxis stability of plankton chains (left axis) and the percentage of fluid inertia effect in the global gyrotactic stability (right axis). Gyrotaxis stability of fluid inertia, bottom-heaviness and the global stability are defined as $1/2T_{inert}$, $1/2B$, and $1/2T_{global}$, respectively.

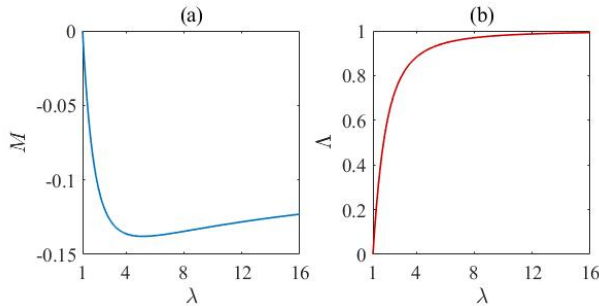


FIG. 8. Evolution of shape factors (a) M and (b) $\Lambda = (\lambda^2 - 1)(\lambda^2 + 1)$ with aspect ratio λ .

fluid information at Eulerian grid points. Eqs. 1 and 2 are integrated by a second-order Adam-Bashforth scheme similarly to time integration of the fluid phase. The number of particles is 120,000 for each parameter configuration, and the statistics in turbulence are formed over more than 40 uncorrelated time samples.

Physical parameters for plankton chains

In the section of *Fluid inertia effect on bottom-heavy plankton*, we provide modelling of the reorientation time and the swimming velocity for plankton chains. They are based on an estimate (8):

$$B = B^{(1)} \alpha_{\perp} / 6, \quad (13)$$

$$v_{swim} = v_{swim}^{(1)} \lambda^{0.4}, \quad (14)$$

where $B^{(1)} = 5$ s and $v_{swim}^{(1)} = 300 \mu\text{m/s}$ are typical reorientation time and swimming velocity of an isolated cell (4, 8, 39), and α_{\perp} is a function of particle aspect ratio (see Appendix in Pedley & Kessler, 1990 (53)). Settling velocities are calculated from Stokes settling velocity of elongated spheroids using Eq. 3 with density ratio $\rho^* = 1.05$. Figure 7 shows the gyrotactic stability due to fluid inertia and bottom-heaviness as functions of λ . The percentage of fluid inertia effect on the global stability increases monotonously with λ and becomes dominant for $\lambda > 10$.

Definition of constants

The shape factor M in Eq. 5, which is a function of aspect ratio λ (Figure 8), is defined as $M = A' I_{\perp} / C_{\perp}$, where I_{\perp} , C_{\perp} and A' are as follows:

$$I_{\perp} = \frac{1 + \lambda^2}{5} a^2, \quad (15)$$

$$C_{\perp} = \frac{8a^2 (\lambda^4 - 1)}{9\lambda [(2\lambda^2 - 1)\beta - 1]}, \quad (16)$$

$$\text{with } \beta = \frac{\ln(\lambda + \sqrt{\lambda^2 - 1})}{\lambda\sqrt{\lambda^2 - 1}}, \quad (17)$$

where a is the length of semi-minor axis of a spheroid. For elongated spheroids:

$$A' = \frac{5}{6\pi} F_{\beta} \frac{\lambda^3}{\lambda^2 + 1}, \quad (18)$$

with F_{β} defined as:

$$\begin{aligned} F_{\beta} = & - \frac{\pi e^2 (420e + 2240e^3 + 4249e^5 - 2152e^7)}{315 [(e^2 + 1) \tanh^{-1} e - e]^2 [(1 - 3e^2) \tanh^{-1} e - e]} \\ & + \frac{\pi e^2 (420 + 3360e^2 + 1890e^4 - 1470e^6) \tanh^{-1} e}{315 [(e^2 + 1) \tanh^{-1} e - e]^2 [(1 - 3e^2) \tanh^{-1} e - e]} \\ & - \frac{\pi e^2 (1260e - 1995e^3 + 2790e^5 - 1995e^7) (\tanh^{-1} e)^2}{315 [(e^2 + 1) \tanh^{-1} e - e]^2 [(1 - 3e^2) \tanh^{-1} e - e]}, \end{aligned} \quad (19)$$

where $e = \sqrt{1 - \frac{1}{\lambda^2}}$.

For more details, readers can refer to references (27–29) for the physical meaning of these parameters.

ACKNOWLEDGMENTS

This work was supported by the National Natural Science Foundation of China (Grant No. 11702158 and 11911530141). JQ and LZ acknowledge the support from the Institute for Guo Qiang of Tsinghua University (Grant No. 2019GQG1012).

[1] Y. Sekerci and R. Ozarslan, Chaos, Solitons & Fractals **132**, 109532 (2020).

[2] X. Wang, J. R. Christian, R. Murtugudde, and A. J. Busalacchi, Geophysical Research Letters **32** (2005), 10.1029/2004GL021538.

[3] J. G. Park, M. K. Jeong, J. A. Lee, K.-J. Cho, and O.-S. Kwon, Phycologia **40**, 292 (2001).

[4] T. J. Smayda, Progress in Oceanography **85**, 71 (2010).

[5] T. Katajisto, M. Viitasalo, and M. Koski, Marine Ecology Progress Series **163**, 133 (1998).

[6] G. Basterretxea, J. S. Font-Muñoz, and I. Tuval, Frontiers in Marine Science **7**, 185 (2020).

[7] O. Pundyak, Oceanologia **59**, 108 (2017).

[8] S. Lovecchio, E. Climent, R. Stocker, and W. M. Durham, Science Advances **5**, 7879 (2019).

[9] W. M. Durham, J. O. Kessler, and R. Stocker, Science **323**, 1067 (2009).

[10] A. Sengupta, F. Carrara, and R. Stocker, Nature **543**, 555 (2017).

[11] W. M. Durham, E. Climent, M. Barry, F. De Lillo, G. Boffetta, M. Cencini, and R. Stocker, Nature Communications **4**, 1 (2013).

[12] F. De Lillo, M. Cencini, W. M. Durham, M. Barry, R. Stocker, E. Climent, and G. Boffetta, *Physical Review Letters* **112**, 044502 (2014).

[13] C. Zhan, G. Sardina, E. Lushi, and L. Brandt, *Journal of Fluid Mechanics* **739**, 22 (2014).

[14] K. Gustavsson, F. Berglund, P. R. Jonsson, and B. Mehlig, *Physical Review Letters* **116**, 108104 (2016).

[15] M. Borgnino, G. Boffetta, F. De Lillo, and M. Cencini, *Journal of Fluid Mechanics* **856** (2018).

[16] S. Lovecchio, F. Zonta, C. Marchioli, and A. Soldati, *Physics of Fluids* **29**, 053302 (2017).

[17] M. Mashayekhpour, C. Marchioli, S. Lovecchio, E. N. Lay, and A. Soldati, *Advances in Water Resources* **129**, 328 (2019).

[18] C. Marchioli, H. Bhatia, G. Sardina, L. Brandt, and A. Soldati, *Physical Review Fluids* **4**, 124304 (2019).

[19] J. O. Kessler, *Journal of Fluid Mechanics* **173**, 191 (1986).

[20] S. O’Malley and M. Bees, *Bulletin of Mathematical Biology* **74**, 232 (2011).

[21] A. M. Roberts, *The Biological Bulletin* **210**, 78 (2006).

[22] A. Bérut, H. Chauvet, V. Legue, B. Moulia, O. Pouliquen, and Y. Forterre, *Proceedings of the National Academy of Sciences* **115**, 5123 (2018).

[23] D. P. Häder, M. Lebert, P. Richter, and M. Ntefidou, *Advances in Space Research* **31**, 2181 (2003).

[24] R. Hemmersbach, D. Volkmann, and D.-P. Häder, *Journal of Plant Physiology* **154**, 1 (1999).

[25] D.-P. Häder, M. Braun, D. Grimm, and R. Hemmersbach, *npj Microgravity* **3**, 1 (2017).

[26] R. Hemmersbach and D. P. Häder, *The FASEB Journal* **13**, S69 (1999).

[27] M. Z. Sheikh, K. Gustavsson, D. Lopez, E. Lévéque, B. Mehlig, A. Pumir, and A. Naso, *Journal of Fluid Mechanics* **886**, A9 (2020).

[28] K. Gustavsson, M. Z. Sheikh, D. Lopez, A. Naso, A. Pumir, and B. Mehlig, *New Journal of Physics* **21**, 083008 (2019).

[29] V. Dabade, N. K. Marath, and G. Subramanian, *Journal of Fluid Mechanics* **778**, 133 (2015).

[30] V. Dabade, N. K. Marath, and G. Subramanian, *Journal of Fluid Mechanics* **791**, 631 (2016).

[31] M. R. Maxey and J. J. Riley, *Physics of Fluids* **26**, 883 (1983).

[32] N. R. Challabotla, L. Zhao, and H. I. Andersson, *Physics of Fluids* **27**, 061703 (2015).

[33] M. Shapiro and M. Goldenberg, *Journal of Aerosol Science* **24**, 65 (1993).

[34] J. Qiu, C. Marchioli, H. I. Andersson, and L. Zhao, *International Journal of Multiphase Flow* **118**, 173 (2019).

[35] M. N. Ardekani, G. Sardina, L. Brandt, L. Karp-Boss, R. N. Bearon, and E. A. Variano, *Journal of Fluid Mechanics* **831**, 655 (2017).

[36] G. B. Jeffery, *Proceedings of the Royal Society of London. Series A* **102**, 161 (1922).

[37] G. A. Voth and A. Soldati, *Annual Review of Fluid Mechanics* **49**, 249 (2017).

[38] M. Borgnino, K. Gustavsson, F. De Lillo, G. Boffetta, M. Cencini, and B. Mehlig, *Physical Review Letters* **123**, 138003 (2019).

[39] M. H. Sohn, K. W. Seo, Y. S. Choi, S. J. Lee, Y. S. Kang, and Y. S. Kang, *Marine biology* **158**, 561 (2011).

[40] J. Titelman, *Marine Ecology Progress Series* **213**, 203 (2001).

[41] J. Titelman and T. Kiørboe, *Marine Ecology Progress Series* **247**, 123 (2003).

[42] F. Carlotti, D. Bonnet, and C. Halsband-Lenk, *Progress in Oceanography* **72**, 164 (2007).

[43] D. Kamykowski, R. E. Reed, and G. J. Kirkpatrick, *Marine Biology* **113**, 319 (1992).

[44] T. Kiørboe and S. Enric, *Marine Ecology Progress Series* **122**, 135 (1995).

[45] T. J. Smayda, *Marine Geology* **11**, 105 (1971).

[46] J. A. Rudjakov, *Marine Biology* **6**, 98 (1970).

[47] D. Lopez and E. Guazzelli, *Physical Review Fluids* **2**, 024306 (2017).

[48] C. Nilsen, H. I. Andersson, and L. Zhao, *Physics of Fluids* **25**, 115108 (2013).

[49] R. Monchaux, M. Bourgoin, and A. Cartellier, *Physics of Fluids* **22**, 103304 (2010).

[50] M. C. Davey and A. E. Walsby, *British Phycological Journal* **20**, 243 (1985).

[51] R. S. Rogallo, *Numerical experiments in homogeneous turbulence*, Vol. 81315 (National Aeronautics and Space Administration, 1981).

[52] S. B. Pope, *Turbulent flows* (IOP Publishing, 2001).

[53] T. J. Pedley and J. O. Kessler, *Journal of Fluid Mechanics* **212**, 155 (1990).